Journal of Applied Polymer Science

Thermal conductivity of polyimide/boron nitride nanocomposite films

Sombel Diaham,[1,2] François Saysouk,[1,2] Marie-Laure Locatelli,[1,2] Boubakeur Belkerk,[3] Yves Scudeller,[3] Rodica Chiriac,[4] François Toche,[4] Vincent Salles[4]

[1]Université de Toulouse, UPS, INPT, LAPLACE (Laboratoire Plasma et Conversion d'Energie), 118 Route de Narbonne-Bât. 3R3, F-31062 Toulouse cedex 9, France

[2]CNRS, LAPLACE, F-31062 Toulouse, France

[3]Université de Nantes, Ecole Polytechnique, IMN (Institut des Matériaux Jean Rouxel), Rue C. Pauc, La Chantrerie, BP 50609, 44306 Nantes, France

[4]Université Lyon 1, UCBL, LMI (Laboratoire des Multimatériaux et Interfaces), 43 Bd du 11 Novembre 1918, 69622 Villeurbanne Cedex, France

Correspondence to: S. Diaham (E-mail: sombel.diaham@laplace.univ-tlse.fr)

ABSTRACT: The thermal conductivity of polyimide/boron nitride (PI/BN) nanocomposite thin films has been studied for two sizes of BN nanofillers (40 and 120 nm) and for a wide range of content. A strong influence of BN particle size on the thermal conduction of PI has been identified. In the case of the largest nanoparticles (hexagonal-BN), the thermal conductivity of PI/h-BN (120 nm) increases from 0.21 W/mK (neat PI) up to 0.56 W/mK for 29.2 vol %. For the smaller nanoparticles (wurtzite-BN), PI/w-BN (40 nm), we observed two different behaviors. First, we see a decrease until 0.12 W/mK for 20 vol % before increasing for higher filler content. The initial phenomenon can be explained by the Kapitza theory describing the presence of an interfacial thermal resistance barrier between the nanoparticles and the polymer matrix. This is induced by the reduction in size of the nanoparticles. Modeling of the experimental results allowed us to determine the Kapitza radius a_K for both PI/h-BN and PI/w-BN nanocomposites. Values of a_K of 7 nm and >500 nm have been obtained for PI/h-BN and PI/w-BN nanocomposite films, respectively. The value obtained matches the Kapitza theory, particularly for PI/w-BN, for which the thermal conductivity is expected to decrease compared to that of neat PI. The present work shows that it seems difficult to enhance the thermal conductivity of PI films with BN nanoparticles with a diameter <100 nm due to the presence of high interfacial thermal resistance at the BN/PI interfaces. © 2015 Wiley Periodicals, Inc. J. Appl. Polym. Sci. **2015**, *132*, 42461.

KEYWORDS: nanostructured polymers; nanoparticles; nanowires and nanocrystals; polyimides; thermal properties

Received 23 October 2014; accepted 5 May 2015
DOI: 10.1002/app.42461

INTRODUCTION

In recent years, thermally conducting polymers have attracted more and more attention because high thermal conductivity is needed for fast dissipation of heat in electronics. A continuous increase in electronic device density and performance has had a significant impact on the dimensions and complexity of the wiring structure for on-chip interconnects[1] and requirements have changed in advanced interlayer dielectrics (ILDs). In the same way, for high-temperature semiconductor device passivation, new electrical insulating polymers are needed which are able to dissipate the heat efficiently during component operation.

Polymers, such as epoxy,[2] polyvinylidene fluoride,[3] polystyrene,[4] and polyimide (PI),[5,6] can be used in electronic systems but low thermal conductivity and a high thermal expansion coefficient can sometimes restrict their further exploitation. PI has been widely investigated as a packaging material and ILDs due to good electrical, thermal, and mechanical properties. In particular, it possesses a low dielectric constant, low loss tangent, high thermal stability, and high storage modulus. However, it suffers from a very low thermal conductivity in the range of 0.1–0.2 W/mK,[7–9] which is a problem if heat dissipation is required.

Several methods allow increasing the thermal conductivity of polymers. One is the dispersion of micrometric inorganic fillers with high thermal conductivity into a polymer matrix to obtain inorganic/polymer composites. This method is very useful, effective, simple, and subsequently low cost.[2,10,11] For example, thermally conducting ceramic microfillers such as aluminum nitride (AlN),[4,6] alumina (Al_2O_3),[12,13] silicon carbide (SiC),[14] mica,[15] glass fiber,[16] and boron nitride (BN)[17] have been used.

Several studies on the thermal conductivity of PI composites have been reported in the literature. Among them, both Wang *et al.*[6] and Xie *et al.*[18] investigated the thermal conduction of PI/AlN (2 μm) composites. Results showed an increase in the conductivity up to 0.8 W/mK for 30 vol % of AlN. On the contrary, Sato *et al.*[19] and Tanimoto *et al.*[20] reported the thermal conductivity of PI/BN submicro- (0.7 μm) and microcomposites (up to 18 μm) with oriented platelet-shaped hexagonal BN (*h*-BN) particles. For similar submicron (0.7 μm) PI/*h*-BN composites and 60 vol % content, Sato *et al.* and Tanimoto *et al.* obtained values of 7 and 1.9 W/mK, respectively. Such a large difference could be explained by the particle orientation process obtained by consecutive lamination and heat pressing of the films. For PI/(AlN + BN) submicron bicomposites, Kuo *et al.* obtained a conductivity of 2.3 W/mK for 60 vol % content.[21] Finally, for random PI/*h*-BN (1 μm) composites, Li *et al.* obtained a lower value of 1.2 W/mK for 30 wt % of *h*-BN.[22]

With the reduction in polymer film thickness to a few microns, the use of submicro- or microfillers is no longer feasible. However, although only a few studies have been led on PI filled with inorganic nanoparticles, this approach seems interesting and more adapted to thin films. In addition, some of the potential uses and limits of reducing the size of the fillers are known. Recently, Shi *et al.* studied the conduction of PI/AlN (100 nm) nanocomposites but obtained only low values: 0.25 W/mK for 10 wt %.[23] Earlier, Chen *et al.* reported measurements on PI/AlN (40 nm) reaching untypically high values of 1.84 W/mK for 50 vol % of nanoparticles.[24] However, in this case, such results can be explained by the fact that the films were obtained by a precipitation method (sedimentation) followed by hot pressing where the nanoparticles were agglomerated (50 μm).

Nowadays, BN nanoparticles appear very attractive due to their higher thermal conductivity compared to Al_2O_3 and lower cost compared to AlN. Moreover, contrary to AlN, which can often have a natural oxidized layer at the particle surface increasing its thermal resistance, BN is not easily oxidized. A second advantage of BN is that it is not electrically conducting compared to metallic particle filling where electric conducting paths can cause trouble. Until now, only Li *et al.* have investigated the thermal conductivity of PI/BN nanocomposites with a particle size around 200 nm.[25] They found a value of 0.47 W/mK for 30 wt % of *h*-BN. However, and even if the enhancement seems to depend on the filler size, no study has been performed for smaller nanoparticle sizes. In addition, no studies modeling the thermal properties of PI/BN nanocomposites exist.

In this study, the thermal conductivity of PI/BN nanocomposite films is investigated for two different BN nanoparticle sizes as a function of the filler volume content. The measurements are performed using an original measurement technique specific to thin films (μm thickness). Finally, the experimental results are analyzed using different theoretical thermal conduction models and some physical parameters are extracted and discussed.

EXPERIMENTAL

Materials

The material used as the host matrix in this study is a PI synthesized from biphenyl tetracarboxylic dianhydride (BPDA) and *p*-phenylene diamine (PDA) precursor monomers. The BPDA/PDA PI has a density of 1.48 g/cm^3. The two monomers are dissolved in *N*-methyl-pyrrolidone (NMP) to form a polyamic acid (PAA) precursor liquid solution with a viscosity of 120 poises.

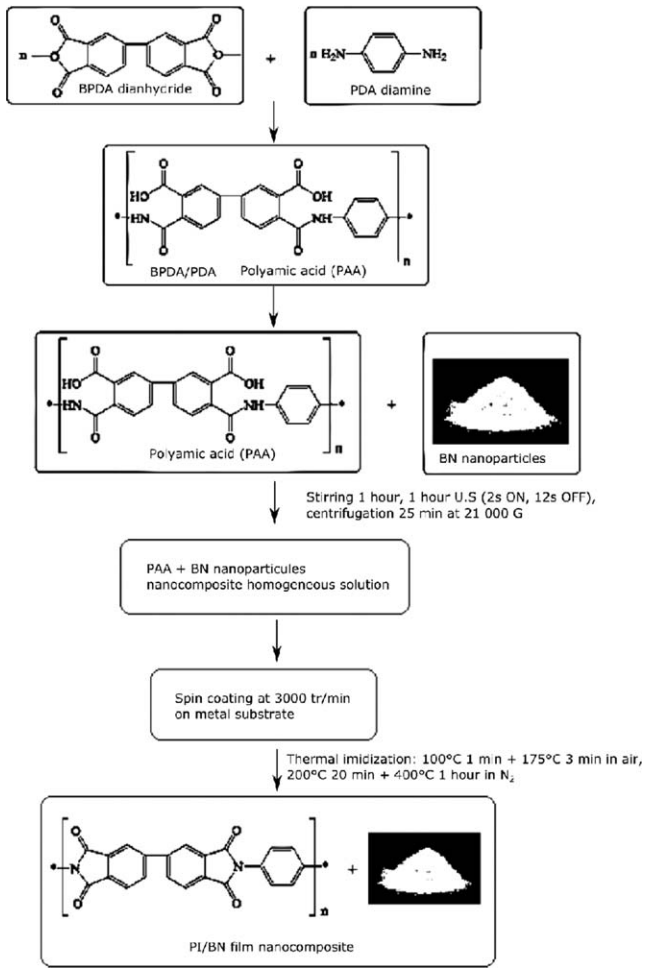

Figure 1. Elaboration process of the PI/BN nanocomposite films.

Two grades of commercial BN nanoparticles with average diameters of 40 and 120 nm were used. The nanofiller characterizations will be given in the following sections.

Preparation of PI/BN Nanocomposites

The preparation of PI/BN nanocomposites is based on direct blending of BN nanoparticles (with different initial wt %) with the PAA precursor solution before dispersing them by sonication. For this critical step of the process, a high-power ultrasonic probe was used to sonicate and disperse the BN nanoparticles in the PAA solution at 200 W for 1 h with a pulse waveform of 2 s "on" and 12 s "off." After dispersion, the PAA/BN solutions had good electrostatic stabilities with high ζ-potential values. A schematic representation for the preparation process is shown in Figure 1.

The PAA/BN solutions were then deposited on metallic substrates (33 × 33 mm^2 stainless steel) using a spin-coating technique at 3000 rpm for 30 s. Substrates were first cleaned and

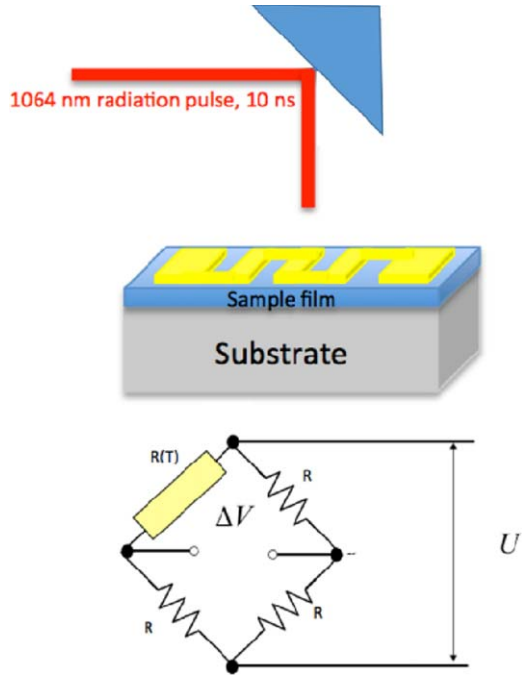

Figure 2. Schemes representing the Au resistor sensor deposited on the film surface and excited by a laser pulse, and the Wheatstone bridge circuit used for measuring the thermal conductivity. [Color figure can be viewed in the online issue, which is available at wileyonlinelibrary.com.]

treated using an adhesion promoter solution. Then, after coating, the polymerization was done by consecutive curing of the nanocomposite films at 100°C for 1 min and 175°C for 3 min in air and then 200°C for 20 min and 400°C for 1 h under nitrogen. The film thicknesses were varied from 2.5 to 5 μm depending on the BN content.

As a consequence of the curing process, where the NMP solvent is evaporated from the coated films, the PI and BN weight ratio is changed. Therefore, the real BN content was evaluated on peeled films, as described below.

Measurements

The crystal structures of the BN nanofillers were investigated by X-ray diffraction (XRD) using a Bruker diffractometer D4 ENDEAVOR on around 1 g of nanopowder.

The volume content of the BN nanoparticles within the PI matrix was evaluated on peeled films by measuring the volume density by helium pycnometry using a Micromeritics Accupyc 1330 setup. Volume contents varied up to 29.2 and 57.3 vol % for the largest and smallest BN nanoparticles, respectively.

Thermal conductivity measurements were carried out using a pulsed photothermal technique developed to determine the thermal properties of thin solid films and coatings.[26–29] A gold (Au) "steamer" thin resistor (thickness 150 nm, strip length 64 mm, width 700 μm), used as a thermal sensor, was deposited by thermal evaporation on the surface of each sample with a total resistance of 20 Ω as shown in Figure 2. To measure the conductivity, the resistor was connected to a Wheatstone bridge compound of three other discrete resistors with low temperature coefficients able to operate up to 400 MHz. Following the sudden temperature increase induced by the absorption of a Nd:YAG laser pulse by the Au resistor sensor, a disequilibrium of the Wheatstone bridge occurs leading to an increase in the balanced voltage ΔV (Figure 2). The wavelength, pulse width, and energy density of the irradiation were 1064 nm, 10 ns, and 0.2 J/cm^2, respectively. The whole circuit was integrated in an electromagnetic protection case and was maintained at constant room temperature. The thermal conductivity was determined by measuring the rate of temperature decrease of the Au resistor sensor due to heat dissipation into the nanocomposite films.

The transient temperature dissipation ΔT above ambient temperature was determined by detecting the unbalanced voltage ΔV of the bridge immediately after the laser pulse irradiation. ΔV was measured with a digital oscilloscope and ΔT was determined as follows:

$$\Delta T(t) = \frac{4\Delta V(t)}{\beta U} \quad (1)$$

where β is the temperature coefficient of the Au layer ($\beta \sim 0.001°C^{-1}$) and U is the DC supply voltage of the bridge. The temperature dissipation ΔT depends on the thermal properties of the film under the Au resistor sensor.

The relation between ΔT and the thermal conductivity λ_{th} has been frequently explained elsewhere and is derived by using a purely diffusive one-dimensional heat transport model of the layered Au/PI–BN/substrate structure with effective thermal properties for each layer and considering adiabatic boundary condition.[26] A genetic algorithm was used for the extraction of λ_{th}, where curve fitting was done over the time interval of 0.1–10 μs. An effective medium approach was considered assuming that each nanocomposite film is homogeneous with a thermal conductivity λ_{th} and a volume heat capacity C_v. The heat capacity for Au and stainless steel was taken as being the bulk values of 0.12 and 0.5 J/g°C, respectively. The thermal conductivity of stainless steel has also been taken into consideration as a bulk value of 14 W/mK.[30]

To determine the volume heat capacity C_v, the specific heat capacity C_p by weight unit of all the PI/BN nanocomposite samples were measured by differential scanning calorimetry – C_p (DSC – C_p) using the sapphire analysis method through a DSC 1 Mettler Toledo setup. All samples were heated from 10 to 400°C at 20°C/min with 5 min at both 10 and 400°C. Aluminum pans of 40 μL each with a pierced lid were used. C_v was thus calculated using the relation $C_v = \rho C_p$, where ρ is the volume density of PI/BN measured by He pynometry using a Micromeritics Accupyc 1330 with a 0.1 cm^3 cell for the films. This cell was used for measurements on the BN nanoparticles. Uncertainties in λ_{th}, C_p, and ρ were evaluated at ±7%, ±3%, and ±0.2%, respectively.

RESULTS AND DISCUSSION

BN Nanopowder Characterization

Figure 3 shows the TEM images of the two kinds of BN nanoparticles used in this study. Figure 3(a) presents a BN-grade with a large distribution of nanofiller diameters. For this material, an average nanoparticle diameter of 120 nm (measured by

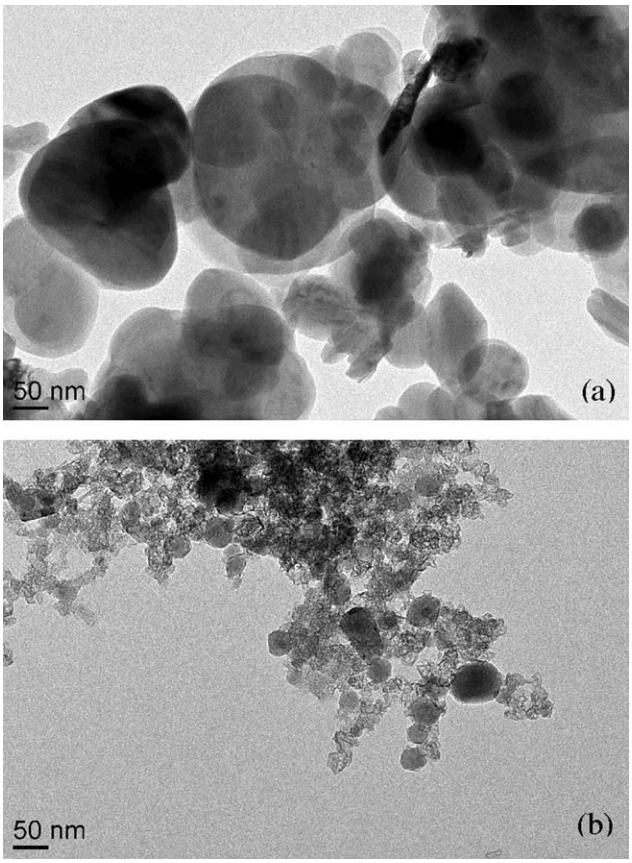

Figure 3. TEM images of (a) *h*-BN and (b) *w*-BN nanoparticles.

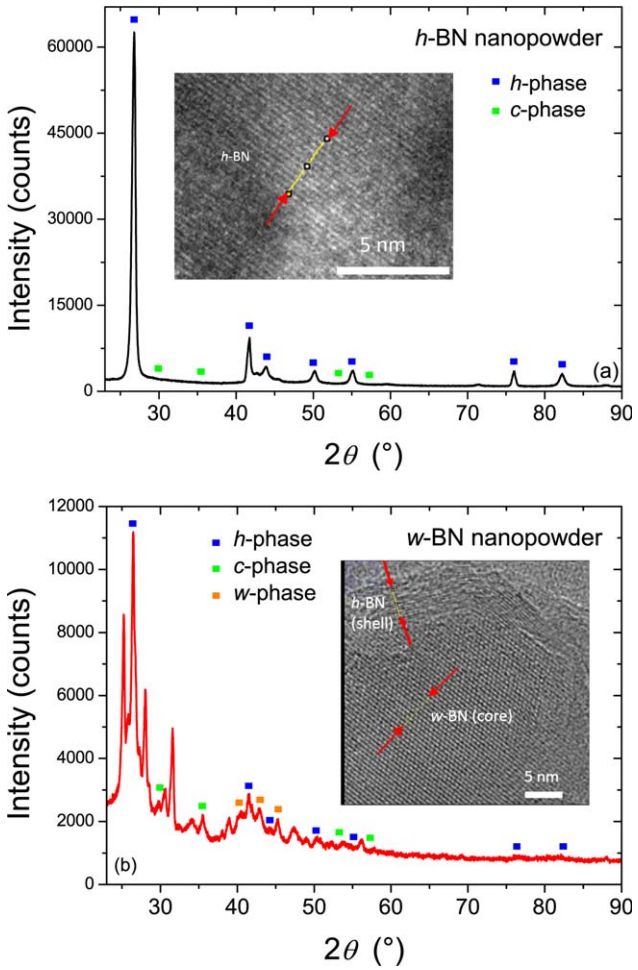

Figure 4. XRD patterns for the (a) *h*-BN and (b) *w*-BN nanoparticles. The square symbols indicate the location of the different crystallographic phases. The inset pictures correspond to high-resolution TEM images for the atomic interplane distance calculations. [Color figure can be viewed in the online issue, which is available at wileyonlinelibrary.com.]

dynamic light scattering) is obtained. Moreover, the nanoparticles show nonhomogeneous geometrical forms with well-defined polyhedron shapes. Figure 3(b) shows the second BN-grade used with a sharper distribution of the nanofiller diameters. In this case, the average nanoparticle diameter is only 40 nm and quasi-spherical shapes are observed.

In order to further investigate the BN nanofillers, both types of nanoparticles were analyzed by XRD and the results are shown in Figure 4. In Figure 4(a), one can observe that only the larger BN nanoparticles (120 nm) present a pure hexagonal crystallographic structure exhibiting all the different hexagonal XRD characteristic peaks (*h*-phase), as identified in the literature.[31] Moreover, the high-resolution TEM image inserted in Figure 4(a) allows the estimation of the average atomic plane distance of 0.32 nm confirming the pure hexagonal structure for this BN-grade,[32] henceforth labeled *h*-BN. Figure 4(b) shows the XRD pattern of the smaller BN nanoparticles (40 nm). In this case, a heterogeneous crystallographic structure is observed composed of both a wurtzite and hexagonal phases (*w*- and *h*-phases).[31,33] In addition, the absence of the cubic characteristic XRD peaks excludes such a crystallographic form.[34] The inset high-resolution TEM image allows us to observe a core–shell structure for these nanoparticles and so estimation of the average atomic plane distances of 0.44 and 0.33 nm within the core and shell, respectively. Such distances highlight a wurtzite structure of the core and a hexagonal structure of the shell.[32] Moreover, some impurities (i.e., Fe_2O_3 and B_2O_3) were identified on this XRD pattern confirmed by elementary XRD (EXRD) measurements coupled to TEM images (not presented here). Henceforth, these nanoparticles will be called *w*-BN due to their mainly wurtzite crystallographic form.

PI/BN Nanocomposite Film Morphology

Figure 5 shows the examples of SEM and TEM images for both PI/*h*-BN and PI/*w*-BN nanocomposite films at the same volume content (21 vol %). On the SEM images, it is possible to observe the impact of the nanoparticles on the roughness of the PI/BN films [Figure 5(a,b)] where in fact, the higher the BN diameter the higher the surface roughness. However, for both kinds of films, the surface appears homogeneous. Roughness values (R_a parameter) of 122 and 27 nm were obtained for the PI/*h*-BN and PI/*w*-BN nanocomposites, respectively, for this filler content. From the TEM images, we can see that the nanoparticles are well dispersed within the films even if some

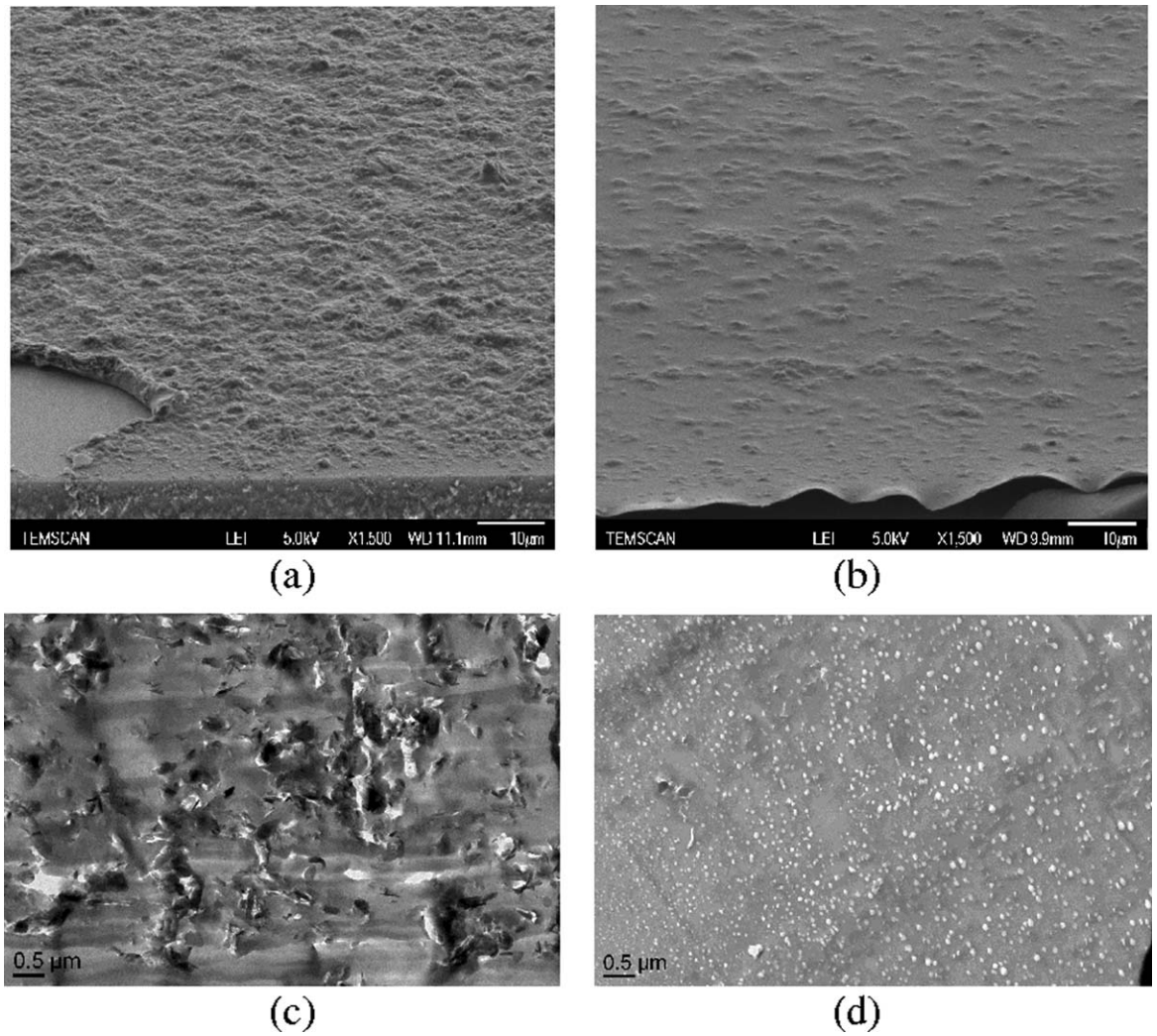

Figure 5. SEM images of (a) PI/*h*-BN and (b) PI/*w*-BN film surfaces at 21 vol % deposited on Si wafers. TEM images of (c) PI/*h*-BN and (d) PI/*w*-BN film cross-sections at 21 vol %.

aggregates appear with sizes between 0.5 and 1 μm for PI/*h*-BN and around 200 nm for PI/*w*-BN.

Volume Density and Heat Capacity

Table I presents the different values of the volume density ρ, specific heat capacity C_p, and volume heat capacity C_v obtained for the PI matrix, *h*-BN and *w*-BN nanofillers and all the PI/BN nanocomposites. For the nanocomposite films, the values of all these parameters are between those of the PI matrix and the BN nanofillers, which is as expected. However, one can observe that the heat capacity increases more rapidly in the case of PI/*h*-BN than PI/*w*-BN at similar filler content. This suggests that the thermal transport is more efficient in PI/*h*-BN due to higher particle size. All these measured parameters have been used for the data modeling for extracting the thermal conductivity of the films that will be discussed more deeply in the following.

Thermal Conductivity of Neat PI

Figure 6 shows the transient evolution of the resistor sensor temperature for the neat PI film during the heat dissipation

Table I. Volume Density, Specific Heat Capacity, and Volume Heat Capacity of the PI Matrix, *h*-BN, *w*-BN, and PI/BN Nanocomposites Obtained at 25°C

	BN (vol %)	ρ (g/cm^3)	C_p (J/gK)	C_v (J/cm^{3}K)
Neat PI	0	1.48	1.09	1.613
h-BN	100	2.30	0.78	1.794
w-BN	100	1.95	0.85	1.658
PI/*h*-BN	2.4	1.51	1.08	1.631
	10.8	1.61	1.04	1.674
	21.0	1.71	0.99	1.693
	29.2	1.80	0.96	1.728
PI/*w*-BN	1.7	1.50	1.08	1.620
	20.6	1.60	1.03	1.648
	42.1	1.70	0.97	1.649
	57.2	1.78	0.94	1.673

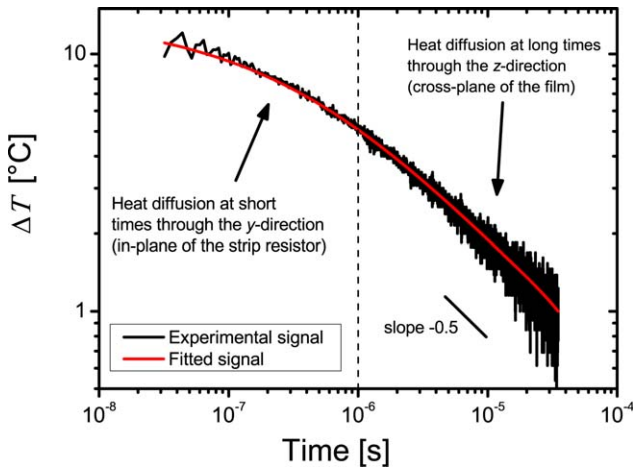

Figure 6. Temperature decrease of the resistor sensor on the neat PI film versus time during the heat dissipation phase following the laser pulse absorption. Slope of −0.5 indicates correct heat transient measurement in the cross-plane direction (in this case, −0.48 is obtained). [Color figure can be viewed in the online issue, which is available at wileyonlinelibrary.com.]

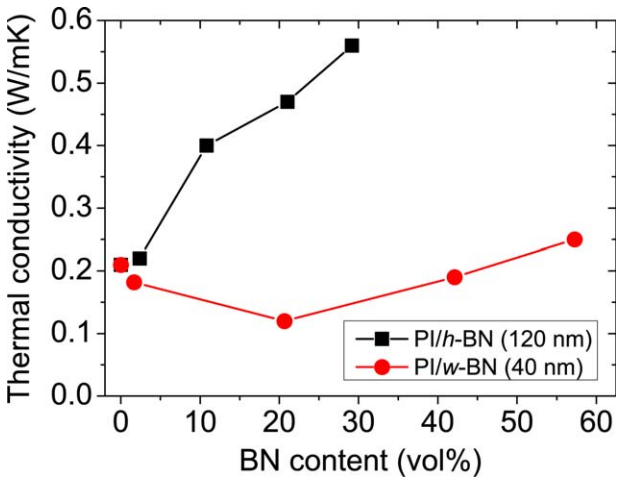

Figure 7. Thermal conductivity of PI/*h*-BN and PI/*w*-BN versus the volume content. [Color figure can be viewed in the online issue, which is available at wileyonlinelibrary.com.]

phase following the laser pulse absorption. A curve obtained by fitting the heat transport model is also presented. More details on the fitting procedure should be found elsewhere.[26,27] One can observe a good agreement between the experimental curve and the model. It has been shown previously by Belkerk *et al.* that such nonlinear evolution of the temperature versus time, particularly at short times below 1 μs, for such thin films with low thermal conductivity reveals that very fast heat diffusion through the *y*-direction of the samples (in-plane) becomes negligible as the strip length/width ratio is greater than 10.[28] In this case, the fact that the strip size is much larger than the film thickness is in favor of the 1D heat transport (cross-plane of the film) and validates the use of the model for such films with low thermal conductivity.

From the fitting procedure, a thermal conductivity of 0.21 W/mK is obtained for the neat PI. Such a value is in very good agreement with the values obtained for PI thin films in the literature using the 3ω method.[1,35]

Thermal Conductivity of PI/BN Nanocomposites

Figure 7 shows the thermal conductivity of PI/*h*-BN and PI/*w*-BN versus the volume content obtained through the same procedure. In the case of PI/*h*-BN, an increase in thermal conductivity is observed with particle volume content. It is enhanced from 0.21 W/mK for the neat PI up to 0.56 W/mK for 29.2 vol % of *h*-BN, which represents an increase of 167%. These values of λ_{th} for PI/*h*-BN are higher than those reported by Li *et al.* (up to 0.47 W/mK) for comparable nanoparticle size.[25] However, such values of λ_{th} remain relatively low compared to those obtained for PI/BN microcomposites which is as expected.[22] This can be explained by the size effect of the nanofillers which allow phonon transport over shorter distances and an increase in the thermal interfacial barrier.

On the contrary, two different behaviors of thermal conductivity are observed for PI/*w*-BN. For a low volume content of *w*-BN below 20 vol %, λ_{th} exhibits an untypical decrease from 0.21 to 0.12 W/mK which are values below those of neat PI. Other authors have already observed such behavior in other nanocomposite materials.[36–40] For a higher volume content of *w*-BN beyond 20 vol %, λ_{th} increases up to 0.25 W/mK for 57.2 vol %. By comparing the results obtained for PI/*h*-BN and PI/*w*-BN nanocomposite films at constant volume content, it is possible to observe the nanoparticle size effect in the improvement of the thermal conductivity. In fact, we observe that for the same volume content, the larger the size of the nanoparticles the greater the thermal conductivity. However, this does not explain the untypical behavior obtained for PI/*w*-BN at low filler content.

The thermal properties of nanocomposite materials are strongly affected by the filler–matrix interface, which introduces a thermal resistance given by eq. (2):

$$R_B = \frac{\Delta\theta}{Q} \tag{2}$$

where $\Delta\theta$ and Q are the temperature difference and the heat flux at the interface, respectively. The interfacial thermal resistance is defined by

$$a_K = R_B \lambda_m \tag{3}$$

where a_K is the Kapitza radius (for which the interfacial thermal property is concentrated on a surface of zero thickness of the particle) and λ_m is the thermal conductivity of the matrix.[37] If the radius a of the nanoparticle is lower than the Kapitza radius a_K, the thermal conductivity of the nanocomposite material λ_c will be lower than λ_m. As R_B depends on the filler size, a_K is also dependent on a. Using this theory, Hasselman *et al.* and Benvensite described how the thermal conductivity in composite materials can be reduced at low concentration of nanoparticles compared to the conductivity of the base matrix.[42,43] Moreover, Every *et al.* and Ordonez-Miranda *et al.* proposed models to explain the reduction of λ_c at high filler content (when it is observed).[37,44] At low filler content, *w*-BN should have a radius ($a = 20$ nm) lower than the Kapitza radius. This could explain

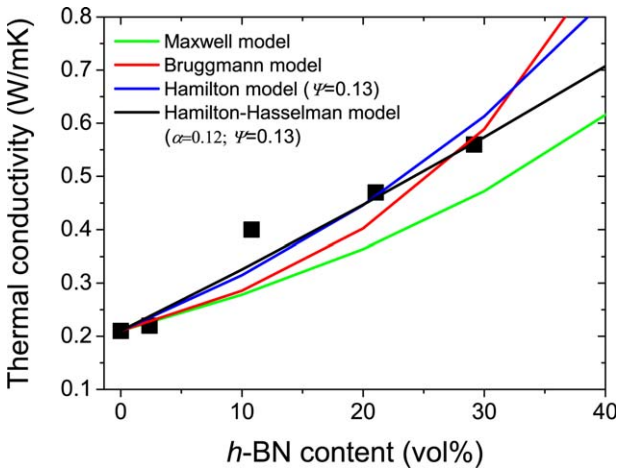

Figure 8. Thermal conductivity modeling for PI/*h*-BN (120 nm). The black dots represent the experimental data of this study. A correlation factor r^2 of 0.95 for the Hamilton–Hasselman model was obtained. [Color figure can be viewed in the online issue, which is available at wileyonlinelibrary.com.]

the decrease in thermal conductivity of PI/*w*-BN below 20 vol %. However, the enhancement of λ_c for contents greater than 20 vol % can be explained by the formation of *w*-BN aggregates (i.e., an increase in effective radius $a > 20$ nm) within the PI matrix inducing a decrease in the specific surface area of the nanofillers (i.e., a decrease in R_B) and the Kapitza radius, simultaneously.

Modeling

Among the different theories for modeling the thermal conductivity of composite materials, the Maxwell and Bruggeman equations are the most used.[45,46] However, they are often unable to describe the conduction behavior of composites for high filler content. Such limitations in those models are related to the fact that filler shape and size are not considered. Hamilton and Crosser proposed a model which considers particle shape.[47] This model is therefore more accurate but it still does not consider particle size. Hasselman *et al.* and Benvensite modeled the size effects of spherical particles by considering an interfacial thermal resistance:[42,43]

$$\lambda_c = \lambda_m \frac{\lambda_p(1+2\alpha)+2\lambda_m+2f[\lambda_p(1-\alpha)-\lambda_m]}{\lambda_p(1+2\alpha)+2\lambda_m-f[\lambda_p(1-\alpha)-\lambda_m]} \quad (4)$$

where λ_p is the thermal conductivity of the particles, f is the volume fraction of particles, and $\alpha = a_K/a$ is the dimensionless parameter. If $\alpha = 0$, there is no barrier resistance.

A combination of the Hamilton and Hasselman models, therefore, allows the effects of both interfacial thermal resistance and particle shape to be described and is given by[48]

$$\lambda_c = \lambda_m \frac{\lambda_p(1+(n-1)\alpha)+(n-1)\lambda_m+(n-1)f[\lambda_p(1-\alpha)-\lambda_m]}{\lambda_p(1+(n-1)\alpha)+(n-1)\lambda_m-f[\lambda_m(1-\alpha)-\lambda_m]} \quad (5)$$

where n is the particle shape factor related to the particle sphericity Ψ with $n = 3/\Psi$. If the particles are spherical, $\Psi = 1$ and $n = 3$, then eq. (5) is equal to eq. (4).

In order to model our experimental results, the thermal conductivities $\lambda_m = 0.21$ W/mK for the neat PI (see measurements above) and $\lambda_p = 30$ W/mK for the BN nanofillers (typical of macroscopic BN properties) were used. For example, in Figure 8, it is possible to observe that the thermal conductivity values of PI/*h*-BN films obtained at high filler content do not fit the Maxwell and Bruggeman equation because these simple models do not take into account the effect of particle shape, or the interparticle interactions. The Hamilton model with a low sphericity ($\Psi = 0.13$ corresponding to the ellipsoidal shape of *h*-BN) seems to better model the results. However, the Hamilton–Hasselman model (with $\Psi = 0.13$ and $\alpha = a_K/a_{h\text{-}BN} = 0.12$) appears as the most suited to describe the thermal conductivity of the PI/*h*-BN films (correlation factor r^2 of 0.95). Considering an average radius $a_{h\text{-}BN} = 60$ nm, the Kapitza radius a_K obtained is around 7 nm. Such a value is below the *h*-BN radius ($a_K < a_{h\text{-}BN}$), meaning that the thermal barrier resistance is confined inside the bulk of the nanoparticles. This leads to the expected, and obtained, enhancement of the thermal conductivity. Moreover, this Kapitza radius value is related to a relatively low interfacial thermal resistance $R_B = 33 \times 10^{-9}$ m^{2}K/W.

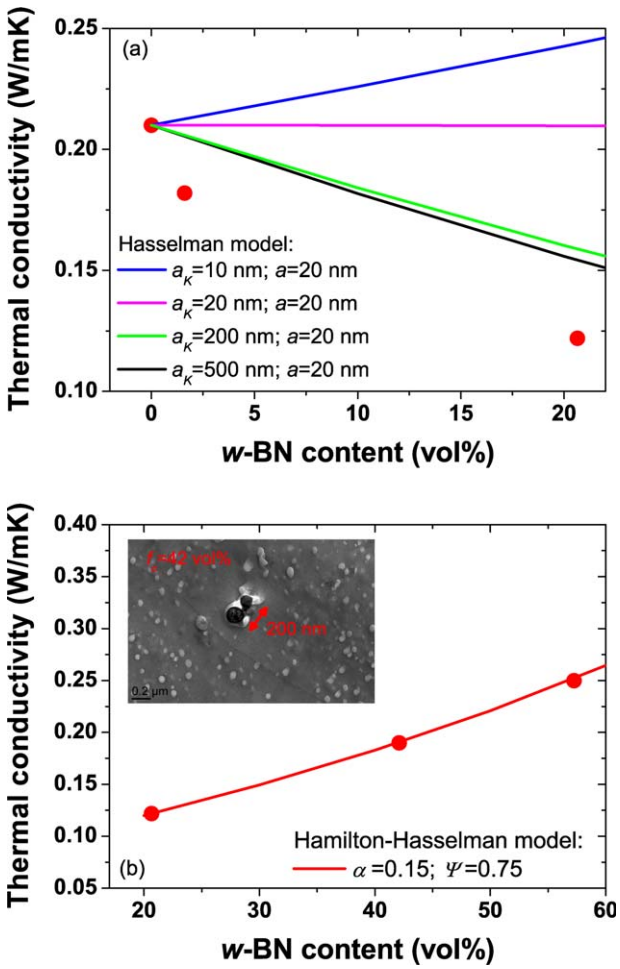

Figure 9. Thermal conductivity modeling for PI/*w*-BN (40 nm) (a) below and (b) above 20 vol %. The red dots represent the experimental data of this study. [Color figure can be viewed in the online issue, which is available at wileyonlinelibrary.com.]

In the case of PI/*w*-BN, the standard theoretical conduction models (Maxwell, Bruggeman, and Hamilton) are not able to

describe the experimental behavior of λ_c. Thus, we have modeled the results using the Hasselman model given by eq. (4) to describe the decrease in thermal conductivity obtained at low concentration of *w*-BN. Figure 9(a) shows the different fits of the thermal conductivity of PI/*w*-BN obtained for different values of Kapitza radius between 10 and 500 nm and when $a_K \leq a_{w\text{-}BN} = 20$ nm, then we should have observed an increase or no change in the thermal conductivity. However, as we observe a decrease in the experimental values up to 20 vol % which means that $a_K > a_{w\text{-}BN}$. Moreover, one can observe a saturation of the fitted curve for $a_K >> a_{w\text{-}BN}$ which also highlights the limits of such models in the description of physical phenomena. Therefore, it is only possible to report here that $a_K > 500$ nm $> a_{w\text{-}BN} = 20$ nm. The minimum value of a_K allows estimation of a higher interfacial thermal resistance $R_B > 2380 \times 10^{-9}$ m^{2}K/W for PI/*w*-BN at the origin of a poor phonon transport in this type of nanocomposite. Such values remain qualitative tendencies in order to bring some orders of magnitude (due to the limit of such model). Another assumption for explaining the deviation should come from the BN thermal conductivity used here, which corresponds to the bulk value (as it is difficult to measure it directly on the nanofillers). Indeed, a better knowledge of this value could allow improving the agreement between experience and model.

For higher filler contents above 20 vol %, one can observe the increase in the mean size of the aggregates of *w*-BN around 200 nm in diameter [Figure 9(b)]. Such aggregates exhibit also a modification of the sphericity of the apparent particles. Considering this value (i.e., $a_{w\text{-}BN} \sim 100$ nm), the increase in the thermal conductivity of PI/*w*-BN has been fitted with the Hamilton–Hasselman model starting from 0.12 W/mK. Values of α and Ψ of 0.15 and 0.75 have been obtained, respectively. The confrontation between TEM images (mean $a_{w\text{-}BN}$ value) and the model (α value) allows deriving an a_K value of 15 nm. In this case, $a_K \ll a_{w\text{-}BN}$; therefore, the thermal conductivity increases again. A lower value of $R_B \sim 100 \times 10^{-9}$ m^{2}K/W is also obtained highlighting that the formation of such small aggregates reduces the interfacial thermal resistance.

Finally, if we consider all the results, this work shows that it seems difficult (probably physically impossible) to enhance the thermal conductivity of PI films with deagglomerated spherical BN nanoparticles with diameters <100 nm even at high filler content due to the presence of high interfacial thermal resistance at the BN/PI interfaces. To overcome such limitations, future research directions should have to focus on improving the interface/interphase coupling between the matrix and the nanofillers or to play with the nanoparticle shape factor (e.g., use of BN nanosheets, nanowires, nanotubes, etc.).

CONCLUSION

The thermal conductivity of polyimide/boron nitride (PI/BN) nanocomposite thin films has been investigated for two sizes of BN nanofillers and as a function of the filler content. The two mean sizes of the nanofillers were of 40 and 120 nm for *w*-BN and *h*-BN, respectively. We have highlighted the strong influence of the BN particle size on the thermal conduction of PI. In the case of the largest BN nanofiller size, the thermal conductivity of PI/*h*-BN (120 nm) increases from 0.21 up to 0.56 W/mK at 29.2 vol % of *h*-BN. For the smaller nanoparticles (*w*-BN), we observed two different behaviors in the thermal conductivity of PI/*w*-BN. First, we observed a decrease to 0.12 W/mK for 20 vol % before an increase for higher filler contents. This phenomenon can be explained by the Kapitza theory and is related to the presence of an interfacial thermal barrier induced by the reduction in size of the nanoparticles. Modeling of the experimental results helped determine the Kapitza radius a_K for both PI/*h*-BN and PI/*w*-BN nanocomposites. Values of a_K of 7 and >500 nm were obtained for PI/*h*-BN and PI/*w*-BN nanocomposite films, respectively. In the case of PI/*w*-BN, the obtained values are higher than the average radius of those nanoparticles (20 nm) in most cases and match the Kapitza features of thermal conductivity. This radius leads to a decrease in the conductivity compared to that of neat PI. Finally, from the results, we have shown that due to the high thermal resistance at the BN/PI interfaces with deagglomerated spherical BN nanoparticles with diameter <100 nm, it is difficult if not impossible to enhance the thermal conductivity of PI films. This information should help in the correct use of these nanoparticles for electronics applications, where an enhancement of the thermal properties is targeted.

TRIBUTE

The authors want to indicate that at the time of writing this article Prof. Yves Scudeller passed away suddenly on June 3rd, 2014. Prof. Scudeller had developed the pulsed photothermal measurement technique and its modeling for obtaining the thermal conductivity on thin films. This work, that would not have been possible without him, is fully dedicated to Prof. Scudeller. The authors are also extremely grateful to him for the many and fruitful scientific discussions they have shared together throughout this collaborative work.

REFERENCES

1. Morgen, M.; Ryan, E. T.; Zhao, J.-H.; Hu, C.; Cho, T.; Ho, P. S. *JOM* **1999**, *51*, 37.
2. Kuo, D.-H.; Chang, C.-C.; Su, T.-Y.; Wang, W.-K.; Lin, B.-Y. *J. Eur. Ceram. Soc.* **2001**, *21*, 1171.
3. Xu, Y.; Chung, D. D. L.; Mroz, C. *Compos. Part A – Appl. Sci. Manuf.* **2001**, *32*, 1749.
4. Yu, S.; Hing, P.; Hu, X. *Compos. Part A – Appl. Sci. Manuf.* **2002**, *33*, 289.
5. Kunman, A.; Kunman, H. *Microelectron. J.* **2000**, *31*, 629.
6. Wang, J.; Yi, X.-S. *J. Appl. Polym. Sci.* **2003**, *89*, 3913.
7. Chen, Y.; Kang, E. T. *Mater. Lett.* **2004**, *58*, 3716.
8. Park, C.; Smith, J. G.; Connell, J. W.; Lowther, S. E.; Working, D. C.; Siochi, E. *Polymer* **2005**, *46*, 9694.
9. He, Q.; Ping, Y. H. *Mater. Chem. Phys.* **2003**, *78*, 614.
10. Xu, Y.; Chung, D. L.; Mroz, C. *Comp. A* **2001**, *32*, 1749.
11. Xiang, F.; Wang, H.; Yao, X. *J. Eur. Cera. Soc.* **2006**, *26*, 1999.

12. Shimazaki, Y.; Hojo, F.; Takezawa, Y. *Appl. Phys. Lett.* **2008**, *92*, 133309.
13. Bujard, P.; Kuhnlein, G.; Ino, S.; Shiobara, T. *IEEE Trans. Compon. Packag. Manuf. Technol. A* **1994**, *17*, 527.
14. Li, L.; Chung, D. D. L. *J. Electron. Mater.* **1994**, *23*, 557.
15. Bajaj, P.; Jha, N. K.; Kumar, A. *J. Appl. Polym. Sci.* **1995**, *56*, 1339.
16. Yen, C. L.; Tseng, H. C.; Wang, Y. Z.; Hsieh, K. H. *J. Appl. Polym. Sci.* **1991**, *42*, 1179.
17. Xu, Y.; Chung, D. D. L. *Compos. Inter.* **2000**, *7*, 243.
18. Xie, S.-H.; Zhu, B.-K.; Li, J.-B.; Wei, X.-Z.; Xu, Z.-K. *Polymer Testing* **2004**, *23*, 797.
19. Sato, K.; Horibe, H.; Shirai, T.; Hotta, Y.; Nakano, H.; Nagai, H.; Mitsuishi, K.; Watari, K. *J. Mater. Chem.* **2010**, *20*, 2749.
20. Tanimoto, M.; Yamagata, T.; Miyata, K.; Ando, S. *Proceedings of the 32nd Jap. Symp. on Thermophys. Prop.*, Yokohama, Japan, **2011**.
21. Kuo, D. H.; Lin, C. Y.; Jhou, Y. C.; Cheng, J. Y.; Liou, G. S. *Polym. Comp.* **2013**, *34*, 252.
22. Li, T.-L.; Hsu, S. L.-C. *J. Phys. Chem. B.* **2010**, *114*, 6825.
23. Shi, C.-Y.; Hao, X.-J.; Zha, J.-W. *J. Adv. Phys.* **2012**, *1*, 78.
24. Chen, X.; Gonsalves, K. E. *J. Mater. Res.* **1997**, *12*, 1274.
25. Li, T.-L.; Hsu, S. L.-C. *J. Appl. Polym. Sci.* **2011**, *121*, 916.
26. Orain, S.; Scudeller, Y.; Garcia, S.; Brousse, T. *Int. J. Heat. Mass. Trans.* **2001**, *44*, 3973.
27. Duquenne, C.; Besland, M-P.; Tessier, P. Y.; Gautron, E.; Scudeller, Y.; Averty, D. *J. Phys. D: Appl. Phys.* **2012**, *45*, 015301.
28. Belkerk, B. E.; Soussou, M. A.; Carette, M.; Djouadi, M. A.; Scudeller, Y. *J. Phys. D: Appl. Phys.* **2015**, *45*, 295303.
29. Achour, A.; Belkerk, B. E.; Ait Aissa, K.; Vizireanu, S.; Gautron, E.; Carette, M.; Jouan, P.-Y.; Dinescu, G.; Le Brizoual, L.; Scudeller, Y.; Djouadi, M. A. *Appl. Phys. Lett.* **2013**, *102*, 061903.
30. Assael, M. J.; Gialou, K. *Inter. J. Thermophys.* **2003**, *24*, 1145.
31. Baraton, M. I.; Boulanger, L.; Cauchetier, M.; Lorenzelli, V.; Luce, M.; Merle, T.; Quintard, P.; Zhou, Y. H. *J. Eur. Ceram. Soc.* **1994**, *13*, 371.
32. Xu, Y.-N.; Ching, W. Y. *Phys. Rev. B* **1991**, *44*, 7787.
33. Soma, T.; Sawaoka, A.; Saito, S. *Mat. Res. Bull.* **1974**, *9*, 755.
34. Mirkarimi, P. B.; McCarty, K. F.; Medlin, D. L. *Mater. Sci. Eng.* **1997**, *R21*, 47.
35. Ju, Y. S.; Kurabayashi, K.; Goodson, K. E. *Thin Solid Films* **1999**, *339*, 160.
36. Nan, C.-W.; Birringer, R.; Clarke, D. R.; Gleiter, H. *J. Appl. Phys.* **1997**, *81*, 6692.
37. Every, A. G.; Tzou, Y.; Hasselman, D. P. H.; Raj, R. *Acta Metall. Mater.* **1992**, *40*, 123.
38. Bai, G.; Jiang, W.; Chen, L. *Mater. Trans.* **2006**,*47*, 1247.
39. Lizundia, E.; Oleaga, A.; Salazar, A.; Sarasua, J. R. *Polymer* **2012**, *53*, 2412.
40. Ordonez-Miranda, J.; Yang, R.; Alvarado-Gil, J. J. *Appl. Phys. Lett.* **2011**, *98*, 233111.
41. Kapitza, P. L. *J. Phys.* **1941**, *4*, 181.
42. Hasselman, D. P. H.; Johnson, L. F. *J. Compos. Mater.* **1987**, *21*, 508.
43. Benvensite, Y. *J. Appl. Phys.* **1987**, *61*, 2840.
44. Ordonez-Miranda, J.; Alvarado-Gil, J. J. *Comp. Sci. Technol.* **2012**, *72*, 853.
45. Fricke, H. *Phys. Rev.* **1924**, *24*, 575.
46. Bruggeman, D. A. G. *Ann. Phys.* **1935**, *24*, 636.
47. Hamilton, R. L.; Crosser, O. K. *Indus. Eng. Chem. Fund.* **1962**, *1*, 187.
48. Jiajun, W.; Xiao-Su, Y. *Comp. Sci. Technol.* **2004**, *64*, 1623.